Electron tunneling through barriers of adjustable width: Role of the image potential and the wetting behavior of Cs by He

M. Zech,[1,*] H. Bromberger,[1] J. Klier,[1,†] P. Leiderer,[1] and A. F. G. Wyatt[2,‡]
[1]*Faculty of Physics, University of Konstanz, Konstanz 78457, Germany*
[2]*School of Physics, University of Exeter, Exeter EX4 4QL, United Kingdom*
(Received 20 March 2008; revised manuscript received 14 July 2008; published 16 September 2008)

Photocurrents from cesium, flowing through gaseous ^{3}He or ^{4}He and also through thin liquid helium films, are investigated as a function of the chemical potential of helium at $T=1.33$ K. At low pressures, the two isotopes behave similarly as the photocurrent is governed by scattering by the gas. At higher pressures, a film of ^{3}He grows on the Cs and forms a tunnel barrier; but for ^{4}He, the film is too thin to form a tunnel barrier below liquid-vapor coexistence. This is because ^{4}He does not wet Cs at this temperature and the finite thickness needed to form a tunnel barrier is larger than the thickness of the thin-film state. ^{3}He enables a continuously variable tunnel barrier thickness to be studied. We show that the image potential is important and confirm that an electron in liquid ^{3}He has a potential energy of 1.0 eV. We find that the thickness d of a helium film is given by $\Delta C_3/d^3=-k_BT\ln(p/p_0)$ for films thicker than approximately three monolayers.

DOI: 10.1103/PhysRevB.78.115113 PACS number(s): 72.40.+w, 73.40.Gk, 67.30.ej, 68.08.Bc

I. INTRODUCTION

The helium-cesium system is very interesting from several points of view, and it gives an opportunity to study some important physical principles in a unique way. The interaction of liquid helium with the surface of Cs is so finely balanced that liquid ^{4}He does not wet Cs below the wetting temperature $T_w=2.0$ K, but liquid ^{3}He does wet Cs. The nonwetting of ^{4}He was predicted by Cheng *et al.*[1] and measured in Refs. 2–4 and reviewed in Refs. 5 and 6. The different behavior of ^{3}He was analyzed in Refs. 7 and 8 and measured in Refs. 9–11. This means we can create films of liquid ^{3}He of variable thickness on Cs. But under exactly the same conditions of temperature and pressure, there should be at most a very thin layer of ^{4}He, of order one monolayer, on the Cs. Also it has been predicted that ^{3}He forms a prewetting layer of three monolayers on Cs.[12]

Besides these interesting properties, Cs has a low electronic work function, $\phi_w=1.8$ eV, which is in fact the lowest among those of all pure metals, so that photoelectrons can be emitted with visible light. This gives the possibility of measuring the electron-tunneling probability under well-defined conditions: If the Cs is illuminated with suitably low-energy photons, the photoelectrons must tunnel through the liquid helium film to escape. As the thickness of the liquid ^{3}He film can be adjusted by changing the pressure, this ^{3}He-Cs system gives the unique opportunity to measure tunneling through a barrier whose thickness can be changed without altering the other conditions.

In this paper we report measurements of the photoemission from Cs in the presence of ^{3}He and ^{4}He atmospheres. At low pressures, ^{3}He and ^{4}He behave the same way. This is in the regime where the adsorbed helium on the Cs does not create a tunneling barrier; we shall see that this is a consequence of the image potential. At higher pressures, we show that a ^{3}He film grows in thickness and forms a tunnel barrier, while the ^{4}He remains in the thin-film state on the Cs. As the emitted photoelectrons still have to propagate through the gas when there is a tunnel barrier, we have to understand how this affects the measured photocurrent and how this effect can be separated from the tunneling. As tunneling depends exponentially on the film thickness, this separation can be clearly made for thicker films; we shall see that for films with thickness >10 Å, the photocurrent is almost wholly governed by the tunneling probability when the electron energy is well below the top of the barrier.

One of the questions that occurs, when trying to calculate electron tunnel barriers, is whether to include the image potential,[13] and if it is to be included, what is its form close to the surface of the metal.[14] Theoretical treatments of scanning tunneling microscopes often do not include the image potential, although its effect is expected to be large.[15] We shall see, from our measurements, that the image potential does have a large effect on the tunnel current and we are able to say that the image potential must be included in the tunnel barrier potential.

We set the context with a few numbers. Our Cs has a work function of 1.9 eV, measured by the cut-off frequency for photoemission. Liquid ^{3}He has an electron potential of 1.0 eV at low pressure.[16] So a photon with energy of 2.2 eV would emit electrons, in the energy range of 0–0.3 eV, into a vacuum. These electrons will have to tunnel through a barrier between 1.0 and 0.7 eV, depending on electron energy, if the helium film is many monolayers thick. Their probability of emission is then greatly reduced. A film 15 Å thick has an average probability of tunneling of 2×10^{-3} for electrons with energy of 0.3 eV. However photons with 3.2 eV energy create electrons with energies of up to 1.3 eV. Some of these electrons will pass over the 1.0 eV barrier and will only be weakly reflected by the helium film.

It has been established by a number of experiments that a Cs surface is not wetted by liquid ^{4}He but is wetted by liquid ^{3}He.[10,11] This isotopic sensitivity is due to the greater zero-point motion of the ^{3}He atoms compared to that of the ^{4}He atoms. This directly causes the number density to be lower in ^{3}He than in ^{4}He. Hence the van der Waals potential between atoms is lower in liquid ^{3}He. A liquid will wet a surface if the bonding of an atom to the surface is stronger than its

 ©2008 The American Physical Society

bonding to the liquid.[5] So, for liquid ^{3}He the bonding of a ^{3}He atom to Cs is stronger than that to the liquid and vice versa for ^{4}He.

Helium bonds strongly to most solids and so usually both liquid ^{3}He and liquid ^{4}He wet most surfaces. So it is fortuitous that the bonding of helium to Cs lies between the bondings in liquid ^{3}He and liquid ^{4}He. The bonding to Cs is unusually weak due to the large orbital of the 6*s* wave function, which keeps the He-Cs atoms far apart. Rb, with its smaller 5*s* orbital, forms a stronger bond with helium than Cs and it seems that ^{4}He only marginally does not wet Rb.[17,18]

We imagine a Cs surface in an evacuated cell at a temperature $T \sim 1$ K, and then add ^{3}He gas to the cell. If there is no prewetting jump, then ^{3}He will condense on the Cs and form a liquid film which will increase continuously in thickness as the vapor pressure of the ^{3}He in the cell increases. The film becomes macroscopically thick at the saturated vapor pressure. If there is a prewetting jump, as predicted in Ref. 12, then the Cs surface remains bare until $\Delta\mu$ increases to -0.2 K, and then the film thickness jumps to three monolayers.[12] After this jump, the thickness continuously increases as $\Delta\mu$ increases.

In contrast, at $T \sim 1$ K, which is well below the wetting temperature $T_w = 2.0$ K for liquid ^{4}He on Cs, when we add ^{4}He gas, relatively few atoms condense on the Cs. The thickness of the ^{4}He film stops growing when it is on the order of one monolayer at $T = 1$ K and very much less at $T = 0.1$ K.[19] This so-called "thin-film" state persists until the saturated vapor pressure is reached, at which a sudden first-order transition to a macroscopically thick film occurs. The thin-film state is that which covers the Cs surface surrounding a macroscopic drop of liquid ^{4}He that is also on the surface. This liquid drop forms a compact shape with a finite contact angle between 48° (Ref. 20) and 25° (Refs. 21 and 22) at $T \ll T_w$, depending on the preparation of the Cs surface. The thin-film state of ^{4}He on Cs has been measured by a number of techniques including quartz microbalance,[4] microscopy,[23] surface plasmons,[24] third sound,[3] ellipsometry,[25] and ^{4}He flow measurements.[19]

Many of the surfaces of Cs, which have been studied, have been made by evaporation and quench condensation of Cs onto metal coated glass or quartz. This technique creates rough Cs surfaces,[26] which makes defining and measuring the ^{4}He film thickness difficult. Most techniques measure an average helium film thickness, which gives a larger value for the film thickness than for a film on a smooth plane surface. This is because liquid ^{4}He preferentially goes to concavities in the surface, due to the stronger binding there, and the surface tension of the liquid ^{4}He makes the top surface of the liquid helium film smoother than the surface of the Cs.

In contrast, electron tunneling through a liquid He film is sensitive to the thinnest regions of the film because the tunneling probability decreases exponentially with distance. Hence, measuring the film thickness by tunneling will give a thickness closer to the value on a smooth flat surface. We will see that the thin-film state of ^{4}He on Cs is too thin to form a tunnel barrier, but the growth of a ^{3}He film can be studied up to a thickness of 15 Å. Beyond that, the tunnel current is so low that it is comparable with the noise in the electrometer measuring the system.

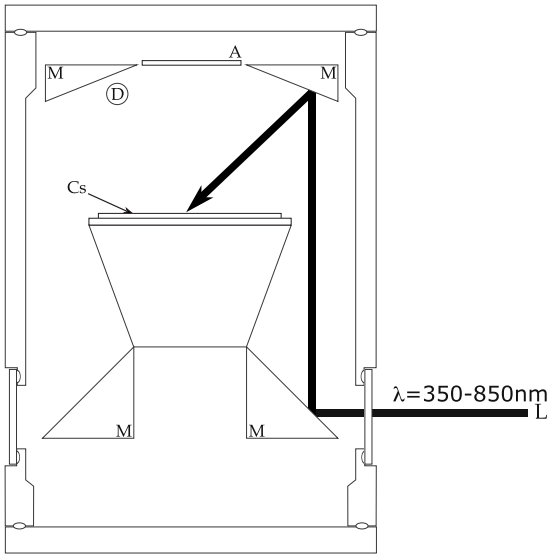

FIG. 1. The experimental cell. The light enters through three windows in the cryostat and one in the cell, and is twice reflected onto the cesium surface. The anode A is typically at 100 V with respect to the photocathode. Cs is evaporated from the dispenser D.

This paper is organized as follows: In Sec. II we describe the experiment and measurements. In Sec. III we discuss the relation between the vacuum photocurrent and the incident light spectrum. In Sec. IV we give a short overview of the behavior of the photocurrent, and in Sec. V we analyze the effect of the vapor on the photocurrent. In Sec. VI we analyze the tunneling through liquid helium films and compare the measured results with a model's calculation. In Sec. VII we draw our conclusions.

II. EXPERIMENTAL METHOD

The measuring cell is shown in Fig. 1. There are two parallel electrodes with a separation of ~20 mm. The top electrode is the anode and consists of a circular glass substrate coated with a thick gold film. The bottom electrode is the photocathode and is a thin cesium film, evaporated *in situ*, onto a gold-plated Dove prism. The anode is held at a potential of typically 100 V with respect to the photocathode. This potential is much greater than the contact potential between the Cs and Au, which is ~3 V. The photocathode is illuminated with monochromatic light from an Acton Research ARC 275 monochromator, which enters the cell through four windows of BK7 glass. The photocurrent is measured with a Keithley 617 electrometer.

The brass cell is inside a Janis ^{4}He bath cryostat and is completely immersed in liquid helium. A thin-walled stainless steel tube, 1 cm diameter and 1 m length, connects the cell to a MKS Baratron 690A13TRB pressure gauge and a turbomolecular pump, both located on top of the cryostat. A thin capillary, soldered to the bottom of the cell, allows helium gas to be let into the cell. The pressure p inside the cell can be controlled in the range of 10^{-6} mbar $< p < 10^3$ mbar. The temperature of the cell is lowered by pumping on the surrounding helium bath. The temperature is

controlled using a small heater and measuring the temperature of the helium bath with a Lakeshore DT-670 thermometer. The temperature can be lowered to 1.3 K. The temperature stability is better than ± 0.5 mK over 12 h. There is a second thermometer, a Cernox, mounted inside the cell, close to the sample.

In a typical experiment, the experimental cell is flushed several times at room temperature with pure 5*n* ^{4}He gas, which has been passed through a cold trap. Then, the turbomolecular pump lowers the pressure inside the cell to $\sim 1 \times 10^{-6}$ mbar. After 24 h of continuous pumping, the cryostat is cooled down. Once the cryostat has been filled with liquid ^{4}He and before the Cs evaporation, the electric potential is applied between the electrodes, and the gold film on the cathode is illuminated. The purpose of this measurement is to prove that no photoelectrons are liberated. This is to be expected as the shortest wavelength, corresponding to photons of 3.5 eV energy, is insufficient to free electrons from the Au film, which has a work function $\phi_w \sim 5$ eV. In addition, this test determines the background noise of our measurement, which turns out to be on the order of 100 fA.

After this procedure, cesium is evaporated *in situ* onto the bottom Au substrate using a SAES Cs getter source. This source uses a chemical reaction, driven by a heating current of up to 9 A, to provide chemically pure cesium. The duration of the evaporation process is roughly 45 min, depending on evaporation speed and current ramping procedure. During this time, the cell is continuously pumped by the turbomolecular pump. In addition, the cell remains completely immersed in liquid helium, which acts as a cryopump and maintains a low pressure inside the cell even though the substrate itself gets heated up to 80 K due to radiation from the cesium source. The film thickness of the Cs film depends on the duration of the evaporation and can be determined by different methods, which give slightly different results. The final thickness is typically 50 nm.

At the end of the evaporation process, after the substrate has cooled down to 4.2 K, the photocurrent is measured once again as function of incident wavelength. The new Cs surface shows a photocurrent, which starts at a photon energy of 1.9 eV, corresponding to the work function of this cesium film. This proves that cesium has been evaporated onto the former gold substrate. The photocurrent depends strongly on the wavelength of the incident light, which is mainly due to the wavelength dependence of the spectrum of the light source in the monochromator. Typically, the maximum current is achieved at an incident light wavelength of about 530 nm. Typical currents are on the order of 10^3 pA, thus being a factor of 10^4 higher than the noise level of the experimental system and the electrometer. The spectral resolution of the photocurrent is given by the monochromator settings and the corresponding linewidth of the emitted light. In our experiment, the full width at half maximum (FWHM) of the emitted light is ~ 15 nm.

In order to measure the wavelength (λ_p) dependence of this photocurrent, the monochromator is swept from 350 to 850 nm and back at a speed of 100 nm/min. This sweep time is well below the response time of the electrometer; hence the electrometer can respond to any change in photocurrent sufficiently quickly. The spectral output of the monochromator was measured, separately, with an Ocean Optics 2000 spectrometer.

After this, the fridge is cooled down to a temperature of 1.33 K, at which the photocurrent can be measured as a function of the wavelength of the incident light at different pressures in a stable temperature environment. The pressure can be changed by slowly letting gas flow through the long capillary, which connects the experimental cell with a flow meter, a nitrogen cold trap, and a 5*n* ^{4}He or ^{3}He gas cylinder. Typically, the pressure inside the cell is increased by a gas flow of roughly 0.5 cc/min at room temperature. The capillary is spiraled through the helium bath, so the gas is cooled to approximately the temperature of the helium bath. However, to ensure thermal equilibrium, the gas flow is turned off once a suitable pressure inside the cell is achieved and only after a typical delay of 15–30 min is the photocurrent measured. A measurement of the forward and backward sweep of the incident light frequency is made to verify the reproducibility of the recorded data. This procedure is repeated at several pressures until saturation is reached, as measured by the pressure gauge on top of the cryostat. These experiments are repeated for both the ^{3}He and ^{4}He isotopes.

The film of liquid helium on the anode does not impede the electron collection by the anode under steady-state conditions. This is because when low-energy electrons are initially impeded by the potential barrier due to the liquid helium, they will accumulate on its surface and create an electric field across the liquid film such that the potential barrier becomes negligibly thin. The net effect, in the steady state, is that the potential drop across the gas is decreased but all the electrons are collected.

To show that the power of the incident light is not sufficient to locally heat the substrate and thus change the thickness of the adsorbed film, we measured the adsorbed helium film thickness by means of surface-plasmon resonance spectroscopy under different light intensities. No heating was seen with an incident power of 100 μW at 630 nm, illuminating a spot of roughly 5×5 mm^2 on the surface of the cesium film.

III. VACUUM PHOTOCURRENT

In this section we examine how well we can explain the photocurrent measured in a vacuum as a function of photon energy ϵ_p in terms of the incident light spectrum. There are a number of steps and the effect of some processes can only be approximated.

A fraction R of the light incident on the Cs will be reflected. We use $R(\epsilon_p)$ calculated from the measured optical absorption.[27]

As the Cs film is thin, only ~ 50 nm thick, a fraction $F(\epsilon_p)$ of the light that enters the Cs will be absorbed by it. The remainder will pass through the Cs and be absorbed by the underlying thick Au film. Any electrons excited by the light in the Au, which go into the Cs, will be scattered at the Au-Cs interface. We assume that the energy of these electrons is reduced so much that they will not have a high enough energy to leave the Cs and go into the vacuum. The light intensity, through the Cs, decreases as $I/I_0 = \exp(-z/\delta)$,

where the intensity decay length δ is given by

$$\delta = \frac{\lambda_0}{4\pi}\left[\frac{2}{(\epsilon_1^2+\epsilon_2^2)^{1/2}-\epsilon_1}\right]^{1/2}, \quad (1)$$

where λ_0 is the wavelength in vacuum and ϵ_1 and $-\epsilon_2$ are the real and imaginary parts of the dielectric function of Cs, $\epsilon = \epsilon_1 - i\epsilon_2$. The energy absorbed in a Cs film of thickness z_0 is $I_0[1-\exp(-z_0/\delta)]$; hence

$$F(\epsilon_p) = 1 - \exp(-z_0/\delta). \quad (2)$$

We calculate $F(\epsilon_p)$ from the measured complex refractive index of Cs.[27] $F(\epsilon_p)$ varies from 0.719 to 0.371, and $1-R(\epsilon_p)$ varies from 0.307 to 0.950, as the photon energy goes from $\epsilon_p = 1.84$ eV to $\epsilon_p = 3.40$ eV.

Photons absorbed in the Cs will excite electrons from the conduction band in the energy range of $E_F - \Delta E$ to E_F, where ΔE is given by[28]

$$\Delta E = E_F - \frac{(\epsilon_p - \beta G^2)^2}{4\beta G^2}, \quad (3)$$

where $\beta = \hbar^2/2m_e$ and G is the reciprocal lattice vector in Cs; $G_{110} = 2.28k_F$ (Ref. 27) and $\beta k_F^2 = 1.59$ eV. For example, $\Delta E = 0.48$, 0.58, 0.69, and 0.78 eV for $\epsilon_p = 2.3$, 2.5, 2.8, and 3.1 eV, respectively. We see that ΔE is greater than $\epsilon_p - \phi_w$ at low ϵ_p, but less at higher ϵ_p. Some of the excited electrons will go directly into the vacuum—the direct process. Other excited electrons will scatter with equilibrium electrons and then reach the Cs-vacuum interface with reduced energy. Some of these electrons will go into the vacuum—the indirect process. Due to the two processes, there will be escaping electrons in the energy range $0 < \epsilon < \epsilon_p - \phi_w$, where the vacuum energy is taken as zero.

In the absence of measurements on low-energy electrons emitted from cesium, we make the simplifying assumption that a photon creates excited electrons in the Cs, with a uniform number per unit energy in the range of E_F to $E_F + \epsilon_p$, and hence creates escaping electrons, with a uniform number per unit energy in the energy range of $0 < \epsilon < \epsilon_p - \phi_w$. Measurements on potassium[29] show that this is a reasonable first approximation, although there is a minimum corresponding to $E_F - \Delta E$. Hence the fraction of excited electrons in the Cs, with $\epsilon > 0$, is $(\epsilon_p - \phi_w)/\epsilon_p$.

The spectrum from the monochromator, $S(\lambda_p)$, is converted to an intensity $I_p(\omega)$ by noting that $S(\lambda_p)d\lambda_p = I_p(\epsilon_p)d\epsilon_p$. Hence $I_p(\epsilon_p) \propto S(\lambda_p)/\epsilon_p^2$. The incident photon flux is then $I_p(\epsilon_p)/\epsilon_p$ and the absorbed photon flux Φ_a is

$$\Phi_a = [1 - R(\epsilon_p)]F(\epsilon_p)I_p(\epsilon_p)/\epsilon_p. \quad (4)$$

Hence the vacuum current i_0 is given by

$$i_0 = \eta[1 - R(\epsilon_p)]F(\epsilon_p)I_p(\epsilon_p)\frac{(\epsilon_p - \phi_w)}{\epsilon_p^2}e, \quad (5)$$

where η is the quantum efficiency and e is the electronic charge. The quantum efficiency is very low. We estimate that one electron is detected for every $\sim 10^4$ photons incident on the Cs. However for this paper the value of η is immaterial as we are only discussing relative photocurrents.

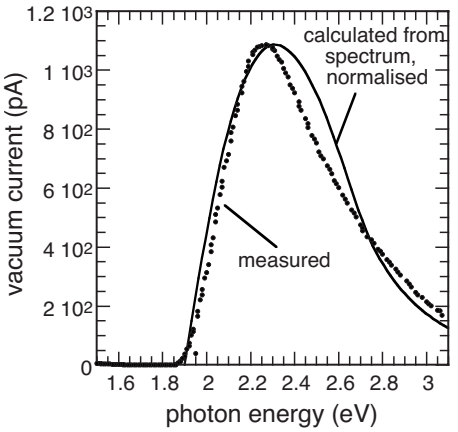

FIG. 2. The measured (dashed line) and calculated vacuum currents (solid line), normalized at the peak, as a function of photon energy.

We show the calculated and measured vacuum currents as a function of photon energy in Fig. 2. The calculated curve is normalized to the same peak height as that of the measured one. We see in Fig. 2 that the measured spectrum is significantly narrower than the calculated one. The normalized calculated current in the range of 2.3 eV $< E <$ 2.7 eV is up to $\sim$20% larger than the measured one. It appears that higher-energy photons are less effective at creating free electrons than lower-energy photons. Most likely the assumed emitted spectrum and emitted fraction of the photoexcited electrons are not quite correct. The spectrum could be measured in a future experiment, using a retarding potential in front of the anode.

IV. OVERVIEW OF THE PHOTOCURRENT WITH HELIUM

The photocurrent is affected by the helium in two ways: by the vapor and by any liquid film that forms on the Cs surface. These two effects can be seen in Fig. 3, where we have plotted i/i_0, where i_0 is the current emitted into a vacuum, as a function of the difference in chemical potential $\Delta\mu$, measured from the value at liquid-vapor coexistence. It is calculated from

$$\Delta\mu = k_B T \ln(p/p_0), \quad (6)$$

where p and p_0 are the vapor pressure and saturated vapor pressure, respectively.

We see in Fig. 3 that i/i_0 initially slowly decreases as $\Delta\mu$ increases, for both isotopes of helium. Nearer to liquid-vapor coexistence, i/i_0 decreases rapidly. For ^{3}He this begins around $\Delta\mu = -0.6$ K, while for ^{4}He it is at $\Delta\mu \sim 0$. The slow decrease in i/i_0 is due to scattering of the photoelectrons by the atoms in the vapor, and the fast decrease is due to tunneling through the liquid helium film on the Cs. We see immediately that ^{4}He does not form a tunnel barrier until a liquid film starts growing at liquid-vapor coexistence. Thus, the behavior of the photocurrent clearly distinguishes between the nonwetting behavior of ^{4}He on Cs and the wetting behavior of ^{3}He on Cs.

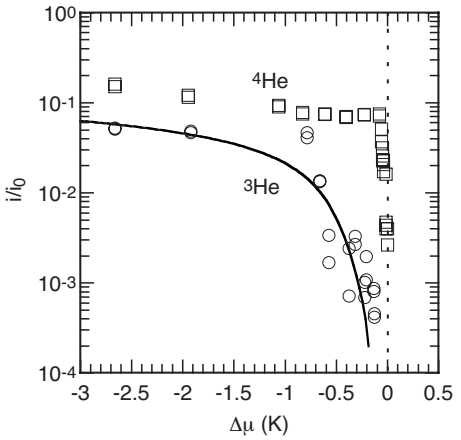

FIG. 3. The photocurrent relative to the vacuum current is shown as a function of chemical potential, measured from liquid-vapor coexistence, for ^{3}He and ^{4}He. The photon energy is 2.2 eV. The slow decrease in photocurrent at low chemical potential is due to scattering in the vapor, and the fast decrease is due to tunneling through a liquid film. It can be seen that a liquid ^{3}He film grows on the Cs well below liquid-vapor coexistence, but for ^{4}He it only grows at liquid-vapor coexistence. The dashed line is calculated from Eqs. (18) and (21) with $\alpha=20$.

Also in Fig. 3, we see that there is no sign of a prewetting jump in the ^{3}He data at $\Delta\mu=-0.2$ K,[12] but this is to be expected at the relatively high temperature of 1.33 K. The solid line for ^{3}He in Fig. 3 is calculated from the theory which combines vapor scattering and tunneling, as will be explained later.

V. EFFECT OF THE VAPOR

In this section we discuss the effect of ^{3}He and ^{4}He gas on the photocurrent. When helium gas is added to the cell, the photocurrent decreases due to the scattering by the vapor. The ^{4}He is in the thin-film state on the Cs and does not form a tunnel barrier, as we shall see later, and so there is only the effect of the vapor for $\Delta\mu<0$. For ^{3}He the effect of the vapor is only dominant at $\Delta\mu<-1$ K.

A photoelectron injected into a gas has a high probability of being backscattered and returned to the photocathode. Thomson[30] proposed that the electrons could be treated as a classical gas within the atom gas. Hence the electron flux in any direction is $nc_1/\sqrt{6\pi}$, where n is the electron number density and c_1 is the root-mean-square velocity. The net electrical current i when there is an atom gas is given by

$$i = i_0 - \frac{1}{\sqrt{6\pi}} n c_1 e, \tag{7}$$

as all backscattered electrons go back into the photocathode. In the atom gas far away from the photocathode, the current is given by $n\mu\Xi$, where μ is the electron mobility and Ξ is the electric field. Putting $n=i/\mu\Xi e$ into Eq. (7), we obtain

$$\frac{i_0}{i} - 1 = \alpha, \quad \text{where} \quad \alpha = \frac{c_1}{\sqrt{6\pi}\mu\Xi}. \tag{8}$$

Using the classical mobility, it was shown in Ref. 31 that

$$\alpha = \frac{\sqrt{\mathrm{KE}_1 \mathrm{KE}_2}}{2\lambda e \Xi}, \tag{9}$$

where λ is the electron mean free path in the atom gas and KE_1 and KE_2 are the kinetic energies of the electrons near and far from the photocathode, respectively. At low pressure, when λ is long, the electrons are not thermalized by scattering with the gas, then[31]

$$\mathrm{KE}_1 = 0.6(\epsilon_p - \phi_w) \tag{10}$$

and

$$\mathrm{KE}_2 = 0.6(\epsilon_p - \phi_w) \quad \text{or} \quad \mathrm{KE}_2 = \frac{2e\Xi\lambda}{\sqrt{2\sqrt{6\pi f}}}, \tag{11}$$

whichever is larger. In the second expression, f is the fraction of energy lost on each collision, $f=2m_e/m_a$, where m_a is the mass of the gas atom or molecule and m_e is the mass of the electron. The first choice of KE_2 is for the case when the electric field is small and the electron retains its emitted energy in the gas, far from the photocathode. The second choice is for the case when the electric field is high and the electron, far from the photocathode, has kinetic energy due to the drift velocity in the electric field. In this latter case, the electron loses its memory of its injected energy.

At high pressures, where λ is short and the electrons are thermalized by the gas, then[31]

$$\mathrm{KE}_1 = \frac{3}{2}k_B T \quad \text{and} \quad \mathrm{KE}_2 = \frac{3}{2}k_B T + \frac{2e\Xi\lambda}{\sqrt{2\sqrt{6\pi f}}}. \tag{12}$$

In this case the kinetic energy from the electric field adds to the thermal energy.

As the gas pressure p is increased, λ decreases, as $\lambda = k_B T/p\sigma$ (where σ is the low-energy electron-atom collision scattering cross section $\sigma=4.99$ Å^2),[32] and there is a gradual transition from a nonthermalized to a thermalized behavior. The change over occurs in the region where[31]

$$\lambda = \left(\frac{3\sqrt{6\pi} m_e \phi_w k_B T}{4 m_a e^2 \Xi^2}\right)^{1/2}. \tag{13}$$

The measured values of $i_0/i-1$ for ^{3}He and ^{4}He are shown as a function of gas number density n in Fig. 4. The similar behaviors of ^{3}He and ^{4}He on Cs, over a large range of gas density, are immediately apparent. At low values of n, when the scattering is due to the gas only, $\ln(i_0/i-1)$ increases slowly as $\ln(n)$ increases, for both ^{3}He and ^{4}He. The ^{3}He data points overlap and continue the line of the ^{4}He points, showing that the scattering by the two gases is very similar. The only difference is in the atomic mass, which occurs in f, and this has a small effect on the current. In this region tunneling is negligible for thin helium films, because below a certain thickness, the film does not create a tunnel barrier. This will be explained in Sec. VI. The behavior changes at higher values of n, with $\ln(i_0/i-1)$ increasing rapidly with increasing n, when the electrons have to tunnel through a film of liquid helium on the Cs. This happens below liquid-vapor coexistence for ^{3}He but at coexistence for ^{4}He; see Fig. 3.

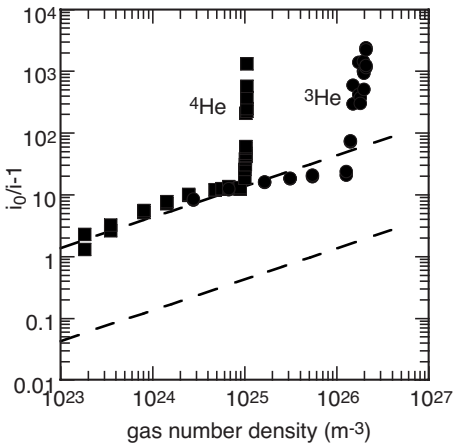

FIG. 4. The function $i_0/i-1$, where i and i_0 are the photocurrents with ^{3}He or ^{4}He and in vacuum, respectively, is shown as a function of gas number density. These are the same data shown in Fig. 3. The upper dashed line is calculated for no thermalization of the electrons, Eq. (10) with KE_2 determined by the applied electric field. The lower dashed line is calculated for complete thermalization, Eq. (12). The sharp rise in $i_o/i-1$ is due to a liquid helium film forming on the Cs, which creates a tunnel barrier for the electrons. This occurs at liquid-vapor coexistence for ^{4}He but below coexistence for ^{3}He.

In Fig. 4, we show the calculated upper and lower lines from Eq. (10) with KE_2 given by the electric field and Eq. (12); the lines are the same for ^{4}He and ^{3}He on this scale. We see that the measured data are well described by the upper line over a large range of gas density n. This indicates that the electrons are not thermalized by scattering by the gas at low gas densities. At higher values of n, the data points for ^{3}He deviate a little from the upper line, showing that the electrons are losing energy by scattering. But we see that they are far from being fully thermalized, as the data points are well above the lower line, which represents full thermalization. At such low temperatures as 1.33 K, it is impossible to have high enough gas pressures, to achieve high enough scattering rates for full thermalization, before condensation occurs.

VI. TUNNELING THROUGH LIQUID HELIUM FILMS

An electron in liquid helium has a potential energy of $\phi_{\mathrm{He}} \sim 1$ eV.[16,33,34] This is the potential before the electron has sufficient time to create a bubble and so lower its energy. This time is on the order of d_0/s, where d_0 is the bubble diameter, 34 Å,[35] and $s=238$ m/s, the velocity of sound in liquid helium; $d_0/s \sim 1.4\times10^{-11}$ s. A typical tunneling time is $[m_e/2(V_0-E)]^{1/2}d$,[36] so the tunneling time when $d=20$ Å is $\sim 10^{-15}$ s. Thus, electrons going through thin films with thickness of ≤ 20 Å do not even begin to create bubbles.

An electron, in the vacuum outside the Cs, will have a potential energy due to its image charge. So the total potential energy of an electron on a film of liquid helium on Cs is

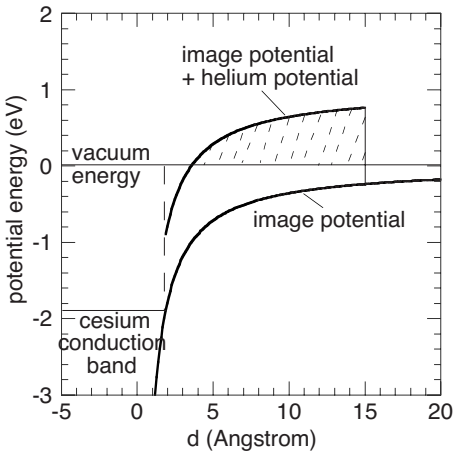

FIG. 5. The electron potential energy as a function of the distance from the Cs surface. The potential is due to the image potential and an additional 1.0 eV where there is a liquid ^{3}He film, shown extending to $d=15$ Å. The tunnel barrier is shown hatched.

$$V(z) = -\frac{e}{16\pi\epsilon_0 z} + \phi_{\mathrm{He}}. \tag{14}$$

Here z is the distance of the electron from the surface of the Cs. The $1/z$ potential cannot be correct for energies below the Fermi energy in the Cs, as electrons in the Cs could otherwise lower their energy by moving into the $1/z$ potential well. We cut off the $1/z$ potential at z_0, where z_0 is given by

$$\frac{e^2}{16\pi\epsilon_0 z_0} = \phi_w, \tag{15}$$

where $z_0=1.9$ Å for $\phi_w=1.9$ eV. The helium atoms cannot approach the Cs surface closer than z_0 due to electron repulsion between the electrons on the He atom and the conduction electrons. This is important when we discuss the film thickness later. The potential is shown in Fig. 5. The shaded area is the tunnel barrier due to a helium film.

The tunneling probability p_t is calculated in the WKB approximation:

$$p_t(\epsilon,d) = \exp\left(-2\int_{z_1}^{d} k dz\right), \tag{16}$$

where k is given by

$$\frac{\hbar^2 k^2}{2m_e} = V(z) - \epsilon \quad \text{for } 0 < \epsilon < V(z). \tag{17}$$

The energy of the electron ϵ is relative to the vacuum energy, which is taken as zero. The end of the film is at $z=d$. We have approximated the prefactor to 1 in Eq. (16).[37]

For the distance along the z direction, where $V(d) > \epsilon > V(z)$, we set $k=0$ so there is no attenuation along this part of the path. When $\epsilon > V(d)$, we assume $p_t=1$; i.e., we ignore the reflection of the electron by the potential because the potential changes slowly on the scale of the wavelength of the electron. When $\epsilon < 0$, there is no possibility of the elec-

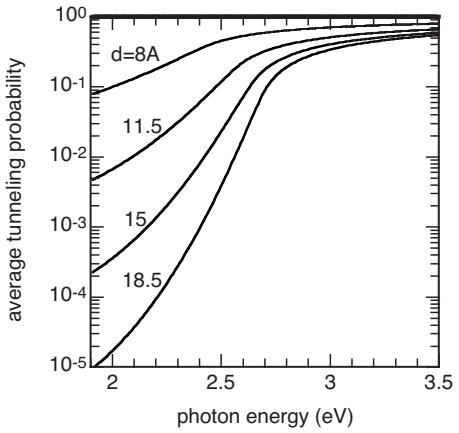

FIG. 6. The average tunneling probability, as defined by Eq. (18) with f constant and $\phi_w=1.9$ eV, is shown as a function of photon energy for $d=8$, 11.5, 15, and 18.5 Å. The curves stop rising when a significant fraction of the electrons can go over the top of the barrier. The energy of the maximum barrier increases with d because of the increasing value of the image potential.

tron escaping the Cs. The average probability $t(\epsilon_p,d)$ of an electron escaping the Cs due to a photon of energy ϵ_p is

$$t=\frac{\int_0^{\epsilon_p-\phi_w} p_t(\epsilon,d)f(\epsilon)d\epsilon}{\int_0^{\epsilon_p-\phi_w} f(\epsilon)d\epsilon}, \tag{18}$$

where $f(\epsilon)$ is the energy distribution of the electrons incident on the barrier.

As discussed in Sec. IV, we assume that a photon with energy ϵ_p creates excited electrons, in the Cs, in the energy range of $E_F<\epsilon<\epsilon_p+E_F$ with a uniform distribution. So $f(\epsilon)$ is a constant which gives $t=t_1$. In Fig. 6 we show t_1 as a function of photon energy for different film thicknesses. It is clear that the electrons from low-energy photons have a much lower probability of escape than the electrons from higher-energy photons.

We now combine this escape probability with the backscattering effect of the gas. Current equation (7) becomes

$$i=i_0t_1-\frac{1}{\sqrt{6\pi}}nce t_2. \tag{19}$$

The average probability t_1 is for the electrons leaving the Cs which have to tunnel out, and t_2 is for the backscattered electrons which have to tunnel into the Cs.

The equation for the current into the gas is unchanged, $n=i/\mu\Xi e$, so we obtain

$$\frac{i}{i_0}=\frac{t_1}{1+\alpha t_2}. \tag{20}$$

When there is no helium, $t_1=t_2=1$, and we regain Eq. (8). When $t_2\ll\alpha^{-1}$, i.e., when the tunneling barrier is thick, then $i/i_0=t_1$; we see that the net photocurrent is independent of the backscattered electrons and hence independent of t_2, and the photocurrent depends only on the tunneling probability out of the Cs.

For intermediate thickness tunnel barriers, we must try to estimate t_2. The electron energy distribution in the gas, near the Cs, is modified by the fact that the electrons leaving the Cs have to tunnel out. The effect of the tunneling is to decrease the injection rate for the low-energy electrons relative to the rate for the higher-energy electrons. So the electron distribution near the Cs is shifted to higher energies. At the high gas pressures which are necessary for a helium film, there will be electron-gas scattering, which will lower the electron energies and shift the distribution to lower energies, in the direction opposite to the effect of the tunneling. We have already seen that scattering only moderately lowers the energy, as the electrons are far from being thermalized by the gas. As the two effects act in opposite directions, we make the approximation that they cancel each other and the energy distribution of the electrons, in the gas near the Cs, is approximately constant, as it is in the Cs. Hence this makes $t_2=t_1$.

Putting $t_2=t_1=t$ into Eq. (20), we obtain

$$\frac{i}{i_0}=\frac{t}{1+\alpha t}. \tag{21}$$

This equation is correct in the two limits of very thin and very thick films, and should apply reasonably well for all thickness tunnel barriers.

In Fig. 3, where we show the measured points of i/i_0 as a function of $\Delta\mu$ for ^{3}He, the line is calculated using Eq. (21). The value of $\alpha=20$ is chosen to give the measured value of i/i_0 due to scattering by the helium gas just before the pressure is high enough to create a measurable tunnel barrier. We see that the calculated line is in agreement with the measured points in the tunneling region.

As the vacuum current calculated from the light spectrum is a poor fit to the measured vacuum current, we calculate the current as a function of ϵ_p, when there is a tunnel barrier, from the measured vacuum current. Again we use $\alpha=20$ for $\epsilon_p=2.2$ eV. If the electrons are fully thermalized then, as we see from Eq. (12), α is independent of ϵ_p. However we assume that α does not vary with ϵ_p even though the electrons are only partially thermalized. The measured and calculated currents, as a function of photon energy, are shown in Fig. 7. The thickness of the films, for the calculation, were chosen to fit the experimental data, and we discuss their values later. But we note here that their values are close to the film thicknesses calculated from $\Delta\mu$.

In Fig. 7, we see that the peak current shifts to higher photon energies as the ^{3}He film thickens. This is a clear sign of tunneling, which most strongly attenuates the lower-energy electrons. The peak of the thinnest film is not shifted much from the vacuum current. This is because the tunneling with $t\sim0.2$ has only a small effect on the current as $t/(1+\alpha t)$ is not very different from $1/(1+\alpha)$ for this value of t. For thicker films, αt in Eq. (20) is smaller, as t decreases rapidly with film thickness for the lower-energy electrons. This causes the peak to shift to higher energies.

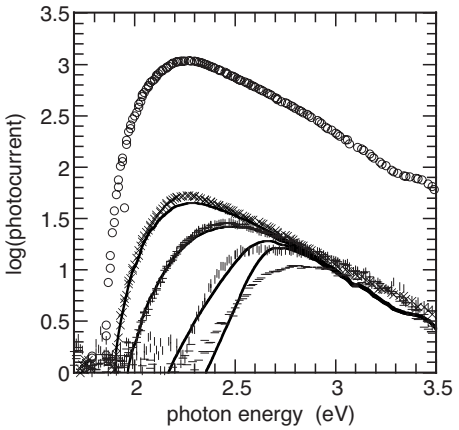

FIG. 7. The measured photocurrent in picoamperes, in vacuum and with liquid ^{3}He films, is shown as a function of photon energy. The film thicknesses calculated from Eq. (22) are 0, 8.7, 10.2, 12.3, and 14 Å. Also are shown are the calculated currents from the model using Eq. (21) with $\alpha=20$ for $d=8$, 11.5, 15, and 17.5 Å, i.e., film thicknesses of 6.1, 9.6, 13.1, and 15.6 Å.

For electrons with energy higher than the top of the potential barrier, there is no attenuation except for the weak reflection, which we neglect. The top of the barrier for $d=15$ Å is 0.8 eV. So for photons with energy $\epsilon_p > \phi_w + 0.8$ eV $= 2.7$ eV, the photocurrent becomes weakly dependent on the photon energy. This behavior can be clearly seen in Fig. 7.

We now compare the thicknesses of the ^{3}He films derived from tunneling and from the chemical potential. The equation for d,

$$\Delta C_3/d^3 = -k_B T \ln(p/p_0), \tag{22}$$

is expected to apply only to liquid films of many monolayers but not to very thick films, where retardation effects may lead to deviation from the first-order van der Waals behavior. The assumptions that the liquid is a continuum and the interfaces are smooth and plane are not expected to apply for films that are only a few monolayers thick. But it is not known at what minimum thickness Eq. (22) ceases to apply.

The ^{3}He film thickness from the tunneling measurements is found by fitting the measured and calculated current as a function of photon energy, as shown in Fig. 7. This gives a value for d. The film thickness is then $d-z_0$, for the reason we discussed earlier, namely, that the Cs electrons will fill the image potential up to the Fermi level. As $z_0=1.9$ Å the three film thicknesses from tunneling are 6.1, 9.6, and 13.1 Å. From the chemical potential, using $\Delta C_3 = 700$ K Å^{-1}, we calculate 8.7, 10.2, and 14 Å. Thus, for the second and third thicknesses, the agreement is better than 10%. For the thinnest film, the thickness is poorly determined by the tunneling, as the current is mainly determined by the gas. The cautious conclusion is that Eq. (22) applies at least down to three monolayers of helium.

The ^{3}He results are consistent with the potential shown in Fig. 6. We now consider the implications of this potential for ^{4}He, which on Cs we expect to be in the thin-film state at $T=1.33$ K. We see from the potential-energy diagram, Fig. 5, that a helium film with $d=5.2$ Å does not create a tunnel barrier for 0.3 eV electrons, i.e., films $< d-z_0=3.3$ Å thick, or about one monolayer thick. This insensitivity to thin helium films is a direct consequence of the image potential. It unfortunately means that tunneling cannot investigate the very thin films expected in the thin-film state at $T<1$ K.

The measurements of the photocurrent when ^{4}He is added to the cell at 1.33 K show no tunneling until the vapor pressure reaches the saturated value. There is at most a thin film on the Cs. Because $t/(1+\alpha t)$ is not sensitive to t until $t<0.1$, we can only say that the thin-film state is less than two monolayers, for all pressures below saturation. This is in agreement with the well established view that ^{4}He does not wet Cs at $T<T_w=2$ K, even if the Cs is formed by quench condensation, which creates a relatively rough surface.[26]

It should be mentioned that if there are areas of capillary condensation of ^{4}He on a rough Cs surface, or micropuddles,[38] where the liquid ^{4}He is several monolayers thick, the current from such areas will be much smaller than from areas where there is only a thin-film state. It should, therefore, be possible to investigate such inhomogeneity by detailed measurements of the photoelectron current and a comparison with measurements which determine the integrated film thickness such as ellipsometry or surface plasmons. We expect the helium coverage and hence the current to show hysteresis when the vapor pressure is increased and then decreased, always with $p<p_0$, when there is capillary condensation.

VII. CONCLUSIONS

We have used photoelectrons to investigate the behavior of liquid ^{3}He and ^{4}He films on Cs. We have shown that the photocurrent is determined by scattering of the electrons in the gas and also by electron tunneling when the liquid film thickness is more than one monolayer.

As we expected, ^{3}He wets the quenched condensed Cs film but ^{4}He does not. This is very clearly shown in Fig. 3, where we see that the photocurrent only drops abruptly, due to tunneling, when the pressure reaches saturated vapor pressure for ^{4}He. This indicates that the Cs has only a thin layer of ^{4}He on it until there is liquid-vapor coexistence. In contrast, for ^{3}He, a large reduction in current, due to the film forming a tunnel barrier, occurs well before the saturated vapor pressure is reached, and the film thickness increases continuously as the chemical potential is increased.

At lower pressures, where there is no tunnel barrier, we see that the photocurrent is explained by scattering in the gas. When this happens, there is no difference between the behaviors of ^{3}He and ^{4}He. At very low pressures the photocurrent asymptotically approaches the theoretical line calculated under the assumption that the electrons are not thermalized by the gas. The electron energy near the photocathode is the emitted energy, and far from the photocathode it is due to the applied electric field. As the pressure is increased, the current drops and departs a little from this line and moves toward, but is far from reaching the line calculated assuming that the electrons are fully thermalized. It appears that the pressure cannot be raised to the value at which full thermal-

ization would occur, because condensation intervenes. This is in contrast to photocurrents through H_2 at room temperature,[31,39] where thermalization is nearly attained at the highest pressures. At its maximum, the scattering by helium gas reduces the photocurrent to 0.05 of the vacuum current for 2.2 eV photons; the reduction increases with photon energy.

We were unable to completely explain the vacuum current as a function of photon energy in terms of the measured light spectrum. We do not know where the problem lies, whether it is in the model of photoemission or in knowing the light spectrum incident on the Cs. The model overestimates the relative vacuum photocurrent at higher photon energies.

At higher pressures but still below saturation, a thin film of liquid ^{3}He forms on the Cs, and photoexcited electrons must tunnel through it to escape. The tunneling process takes much less time than that for an electron bubble to form, so the tunneling electron is surrounded by the usual density of ^{3}He atoms. To model this, the potential barrier has to be defined. We have taken the image potential and added the potential due to the ^{3}He. This potential has been measured for ^{4}He,[16,33,34] and for ^{3}He (Ref. 16) it is 1.0 eV for the liquid density at low pressure. As our Cs had a work function of 1.9 eV, this means that electrons with energy 2.7 eV above the Fermi level in the Cs can go over the top of the potential barrier with $d=15$ Å. We see in Fig. 7 that the current for $\epsilon > 2.7$ eV is independent of photon energy. This is good confirmation for the potential being 1.0 eV for bulk liquid ^{3}He.

The image potential substantially reduces the thickness of the barrier for the thin films we have measured. For example, for $d=15$ Å and 2.2 eV photons, with the image potential the average tunneling probability $t=1.33\times10^{-3}$ and without it $t=9.61\times10^{-7}$. The values of $t/(1+20t)$ are 1.29×10^{-3} and 9.61×10^{-7}, respectively. So the current would be orders of magnitude lower without the image potential, and we could not explain our results if we neglected it. As we have an independent measurement of the thickness of the film which creates the barrier, which is not the case for most barriers, we can calculate the tunnel current. As it corresponds to the measured current, we have the strong conclusion that the image potential must be included in the calculation of the tunnel barrier.

By fitting the calculated photocurrent as a function of photon energy, we are able to estimate the thickness of the helium films forming the tunnel barriers. For the two thickest films, where the tunneling dominates the photocurrent, we find that the values of the thickness are within 10% of the thickness calculated from van der Waals potential. So we draw the cautious conclusion that $\Delta C_3/d^3=-k_BT\ln(p/p_0)$ applies at least down to three monolayers of helium.

The image potential means that there is no barrier for electrons with energy of 0.3 eV for one monolayer of liquid helium. Only lower-energy electrons would be sensitive to one monolayer, which means that it is very difficult to measure a change in photocurrent due to one monolayer. Consequently we are led to the conclusion that the thin-film state of ^{4}He on Cs cannot be investigated by photoelectrons.

Tunneling through ^{3}He films would be better studied without the effect of scattering by the gas. This could be achieved by going to low temperatures, around 50 mK, and controlling the ^{3}He film thickness using a reservoir of ^{3}He film to set the chemical potential. A large area of ^{3}He film can be obtained with a fine powder which can be coated with ^{3}He at higher temperatures and then cooled to $T\sim50$ mK. The prewetting transition predicted for ^{3}He (Ref. 12) and other systems could then be sought. It was not seen in the present work because the temperature was too high.

In the future, more information could be obtained if the spectrum of electron energies were measured at each photon energy, instead of measuring the current integrated over all energies. Again this would best be done without the gas scattering. The electron spectrum would tell us more about the photoemission process and would give more information on the shape of the tunnel barrier. It might be possible to measure the profile of the ^{3}He film so that it could be compared to the detailed calculations.[40]

We see that photoelectrons and tunneling confirms that ^{3}He wets Cs but ^{4}He does not. Electron tunneling gives complementary information on the nonwetting and wetting behaviors of helium films on Cs as it is sensitive to the thinnest regions of the film, whereas a quartz microbalance is sensitive to the thickest layers of the film and optical techniques measure an average film thickness. The thin-film state of ^{4}He on Cs at 1.33 K is certainly less than two monolayers, as otherwise we would see a decrease in the current due to tunneling. Finally we have shown that ^{3}He films on Cs is an excellent model system for studying electron tunneling as the potential barrier is well defined in height and width, and the film thickness and, hence, the barrier width can be altered and measured without changing the rest of the system.

ACKNOWLEDGMENT

This work was supported by the Deutsche Forschungsgemeinschaft under Grant No. KL 1186/3.

*Present address: Department of Physics, Harvard University, 17 Oxford Street, Cambridge, MA 02138, USA.

†Present address: ILK Dresden, Bertolt-Brecht-Allee 20, 01309 Dresden, Germany.

‡a.f.g.wyatt@exeter.ac.uk

[1] E. Cheng, M. W. Cole, W. F. Saam, and J. Treiner, Phys. Rev. Lett. **67**, 1007 (1991).

[2] P. J. Nacher and J. Dupont-Roc, Phys. Rev. Lett. **67**, 2966 (1991).

[3] K. S. Ketola, S. Wang, and R. B. Hallock, Phys. Rev. Lett. **68**, 201 (1992).

[4] P. Taborek and J. E. Rutledge, Phys. Rev. Lett. **68**, 2184 (1992).

[5] E. Cheng, M. W. Cole, J. Dupount-Roc, W. F. Saam, and J. Treiner, Rev. Mod. Phys. **65**, 557 (1993).

[6] J. Treiner, Czech. J. Phys. **46**, 2957 (1996).
[7] C. Carraro and M. W. Cole, Phys. Rev. B **46**, 10947 (1992).
[8] E. Cheng, M. W. Cole, W. F. Saam, and J. Treiner, Phys. Rev. B **46**, 13967 (1992).
[9] G. Tastevin, J. Low Temp. Phys. **89**, 669 (1992).
[10] J. E. Rutledge and P. Taborek, J. Low Temp. Phys. **95**, 405 (1994).
[11] J. Klier and A. F. G. Wyatt, Phys. Rev. B **54**, 7350 (1996); J. Low Temp. Phys. **116**, 61 (1999).
[12] L. Pricaupenko and J. Treiner, Phys. Rev. Lett. **72**, 2215 (1994).
[13] M. C. Payne and J. C. Inkson, Surf. Sci. **159**, 485 (1985).
[14] J. A. Appelbaum and D. R. Hamann, Phys. Rev. B **6**, 1122 (1972).
[15] J. M. Blanco, F. Flores, and R. Perez, Prog. Surf. Sci. **81**, 403 (2006).
[16] J. R. Broomall, W. D. Johnson, and D. G. Onn, Phys. Rev. B **14**, 2819 (1976).
[17] N. Bigelow, P. J. Nacher, and J. Dupont-Roc, J. Low Temp. Phys. **89**, 135 (1992).
[18] J. Klier and A. F. G. Wyatt, Phys. Rev. B **65**, 212504 (2002).
[19] P. Stefanyi, J. Klier, and A. F. G. Wyatt, Phys. Rev. Lett. **73**, 692 (1994).
[20] J. Klier, P. Stefanyi, and A. F. G. Wyatt, Phys. Rev. Lett. **75**, 3709 (1995).
[21] E. Rolley and C. Guthmann, J. Low Temp. Phys. **108**, 1 (1997).
[22] J. E. Rutledge, D. Ross, and P. Taborek, J. Low Temp. Phys. **113**, 811 (1998).
[23] X. Muller and J. Dupont-Roc, Europhys. Lett. **54**, 533 (2001).
[24] S. Herminghaus, J. Vorberg, H. Gau, R. Conradt, D. Reinelt, H. Ulmer, P. Leiderer, and M. Przyrembel, Ann. Phys. (N.Y.) **6**, 425 (1997).
[25] T. McMillan, J. E. Rutledge, and P. Taborek, J. Low Temp. Phys. **138**, 995 (2005).
[26] A. Fubel, M. Zech, P. Leiderer, J. Klier, and V. Shikin, Surf. Sci. **601**, 1684 (2007).
[27] N. V. Smith, Phys. Rev. B **2**, 2840 (1970).
[28] R. Y. Koyama and N. V. Smith, Phys. Rev. B **2**, 3049 (1970).
[29] N. V. Smith and W. E. Spicer, Phys. Rev. **188**, 593 (1969).
[30] J. J. Thomson, *Conduction of Electricity Through Gases* (Cambridge University Press, Cambridge, England, 1928), p. 466.
[31] A. F. G. Wyatt, Phys. Rev. B **75**, 214205 (2007).
[32] R. W. Crompton, M. T. Elford, and A. G. Robertson, Aust. J. Phys. **23**, 667 (1970).
[33] W. T. Sommer, Phys. Rev. Lett. **12**, 271 (1964).
[34] M. A. Woolf and G. W. Rayfield, Phys. Rev. Lett. **15**, 235 (1965).
[35] J. Poitrenaud and F. I. B. Williams, Phys. Rev. Lett. **32**, 1213 (1974).
[36] M. Buttiker and R. Landauer, Phys. Rev. Lett. **49**, 1739 (1982).
[37] V. Rojanski, *Introductory Quantum Mechanics* (Prentice-Hall, New York, 1946).
[38] A. F. G. Wyatt and J. Klier, Phys. Rev. Lett. **85**, 2769 (2000).
[39] N. E. Bradbury, Phys. Rev. **40**, 980 (1932).
[40] E. Krotscheck, Phys. Rev. B **32**, 5713 (1985).